DOI: 10.1002/adma.200700540

Enhanced Optical Absorption Induced by Dense Nanocavities inside Titania Nanorods**

By *Wei-Qiang Han*,* *Lijun Wu*, *Robert F. Klie*, and *Yimei Zhu*

Titania, in particular anatase TiO_2, has been extensively used in photo-electrochemical systems, such as dye-sensitized TiO_2 electrodes for photovoltaics and solar cells, water splitting catalysts for hydrogen generation, and for the creation or degradation of specific compounds.[1] To improve the photoreactivity of TiO_2, several approaches, including doping (extension of its absorption wavelength into the visible region) and metal loading (for an efficient electron–hole separation), have been proposed.[2] Furthermore, theoretical calculations predict a significant enhancement of the optical absorbance in a thin silicon film with nanocavities,[3] which indicates another route to increase the photoreactivity of semiconductors. Nanocavities are isolated entities inside a solid and, hence, are very different from nanopores, which (often being irregular and made from amorphous material) connect together and are open to the surface.[4] Nanocavities in solids are usually made by irradiating the material with neutrons, gas ions, or heavy particles.[5] Here we describe a novel approach to produce dense regular polyhedral nanocavities in TiO_2 nanorods by simply heating the intermediate product $H_2Ti_3O_7$ nanorods in air. We found that these dense nanocavities significantly enhance the optical absorption coefficient of TiO_2 in the near-ultraviolet region, thereby providing a new approach to increasing the photoreactivity of the TiO_2 nanorods, for use in applications related to absorbing photons. An "anti-crystal growth" model is proposed for the formation of "anti-nanopolyhedra", that is, nanocavities.

Our synthesis process consists of two steps. First, the intermediate product, $H_2Ti_3O_7$ nanorods, is produced from a NaOH treatment of anatase TiO_2 particles inside an autoclave at a temperature range of 140 to 180 °C for 2–5 days, subsequently followed by acid washing. This procedure is similar to the ways for making $H_2Ti_3O_7$ nanotubes, TiO_2 nanotubes, or other Ti–O-based 1D nanostructures.[6] X-ray diffraction (XRD) measurements show that the intermediate product is monoclinic $H_2Ti_3O_7$ (Fig. 1a). Transmission electron microscopy (TEM) studies show that most of the intermediate products are straight nanorods with diameters from 15 to 200 nm and lengths up to 10 μm. Very small amounts of short and thin $H_2Ti_3O_7$ nanotubes also exist in the intermediate product. In the second step, the intermediate product, $H_2Ti_3O_7$ nanorods, is heated in air at a temperature ranging from 600 to 720 °C. XRD shows that the final product is single-phase anatase TiO_2 (Fig. 1b), which is in agreement with previous reports.[7]

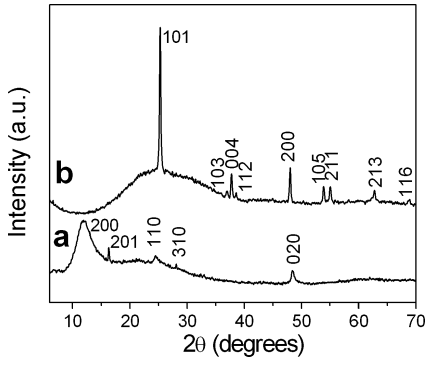

Figure 1. XRD patterns from a) hydrogen titanate nanorods and b) anatase TiO_2 nanorods.

Overall TEM observations show that the nanorods have similar shape and size distributions as those of the intermediate $H_2Ti_3O_7$ nanorods. Most nanorods are single crystals. Interestingly, however, unlike the intermediate $H_2Ti_3O_7$ nanorods, we observe numerous nanocavities inside the TiO_2 nanorods, as shown in the low-magnification TEM image (Fig. 2a). The typical size of the nanocavities is about 10 nm. When the nanorods are viewed along the principle directions, for example, the [100] direction, the nanocavities are seen to have a sharp polyhedral shape, as shown in the high-magnification image with incident beam along the [100] direction (Fig. 2b). The electron diffraction pattern taken from the whole nanorod (inset of Fig. 2b) was indexed as the (100)* pattern of anatase, indicating that the nanorod is still a single crystal phase. Moreover, the nanocavities are rarely present near the edge of the nanorods, even when the nanorod is tilted ±30° along its axis direction. To further confirm the observations, we performed *Z*-contrast imaging and electron energy loss spectroscopy (EELS) analysis in scanning TEM (STEM) mode, as shown in Figure 2c–e. In the *Z*-contrast image,[8] the image intensity is highly sensitive to the thickness and atomic number of the material; the darker areas in the

[*] Dr. W.-Q. Han, Dr. L. J. Wu, Dr. R. F. Klie, Dr. Y. M. Zhu
Center for Functional Nanomaterials
Brookhaven National Laboratory
Upton, NY 11973-5000 (USA)
E-mail: whan@bnl.gov

[**] This work is supported by the U.S. DOE under contract DE-AC02-98CH1088 and LDRD Fund of Brookhaven National Laboratory (to W.H.).

ADVANCED MATERIALS

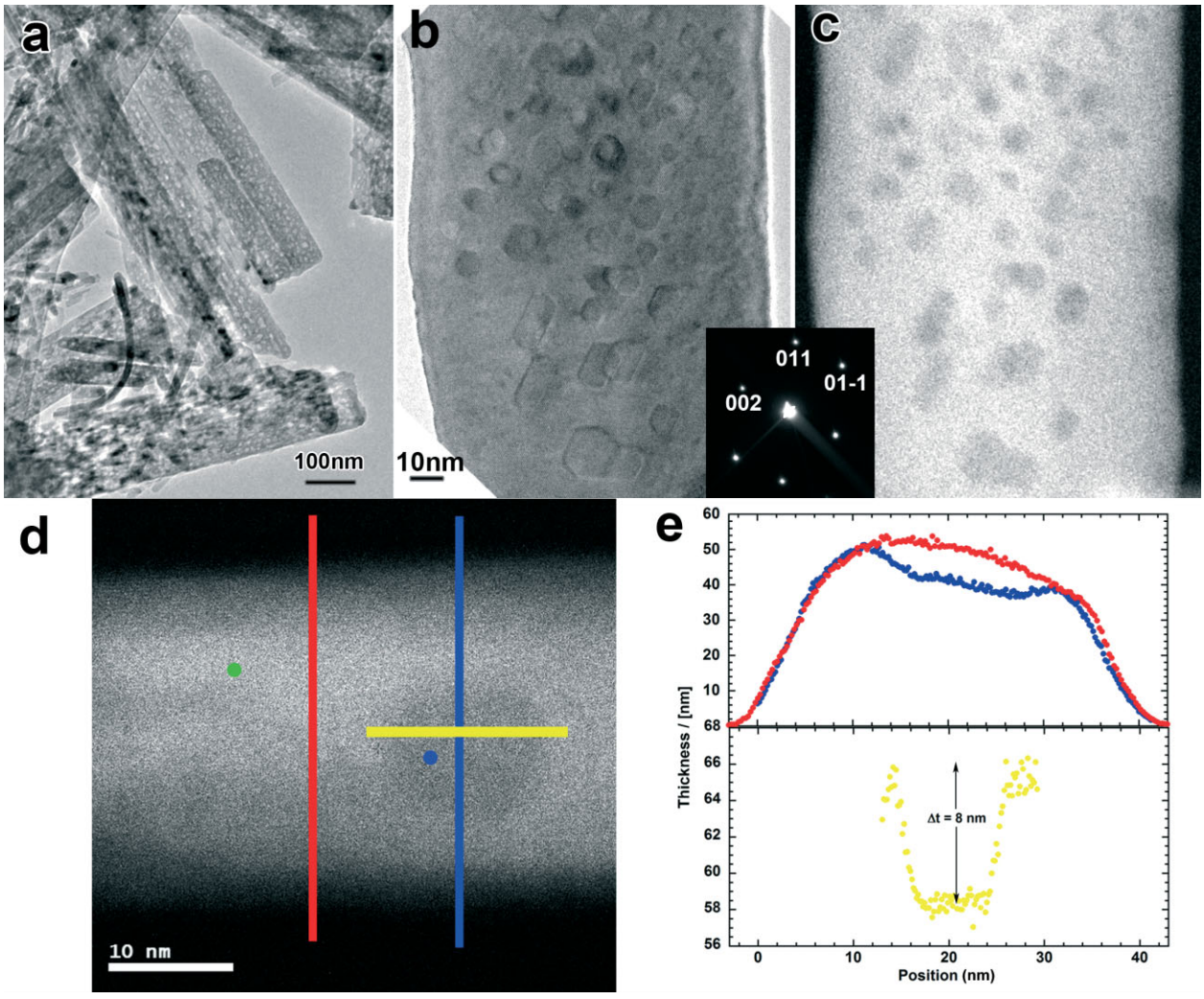

Figure 2. a) Low-magnification TEM image of the TiO_2 nanorods, showing the high density of nanocavities. The image shows that the TiO_2 nanorods have a variety of sizes and that the nanocavities are present in all nanorods. b) High-magnification TEM image of a TiO_2 nanorod, containing many polyhedral nanocavities, viewed along [100] direction. The inset is the electron diffraction pattern taken from the whole nanorod shown in (b). c) *Z*-contrast image from the same nanorod, showing the nanocavities as an area with lower brightness, due to the decreased thickness along the electron-beam direction. d) *Z*-contrast image of one nanocavity with the position of the EELS spectra indicated by the lines and dots. e) Thickness profiles, as calculated from the low-loss EELS spectrum in (d). The two profiles across the nanocavity clearly show the decreased thickness of the nanorod at this position; the depth of the nanocavity was determined to be 8 nm.

TiO_2 nanorod shown in Figure 2c correspond to the nanocavities. Quantitative analysis (Fig. 2e) is provided by EELS analysis of the specimen thickness across the specific dark area shown in Figure 2d. The measured dimensions extracted from the EELS analysis indicates that this particular nanocavity is 8 nm deep and 12 nm wide. More careful analysis of the core-loss EELS spectra reveals that no elements other than Ti and O are present in either the TiO_2 nanorod or the nanocavity, which is consistent with the results from energy-disperse X-ray spectroscopy analysis.

By examining the near-edge fine structure of the Ti L-edge and O K-edge (see Fig. 3), we find that a Ti/O ratio in the area of the nanocavity is 18 % higher than in the "body" of the nanorod. For comparison, an average spectrum, taken at lower magnification is also shown here. In addition, we find that the Ti L_3/L_2 ratio increases at the nanocavities, suggesting a decrease in the Ti valence,[9] which can be due to the decrease in the O stoichiometry of the TiO_2 around the nanocavity.

As a comparison, we also treated the intermediate product, the $H_2Ti_3O_7$ nanorods, at the same experimental conditions except for heating in an argon atmosphere. The product is also nanorods of anatase TiO_2 but without nanocavities. This implies oxygen plays an important role for the formation of nanocavities.

Figure 4a shows a high-resolution TEM image viewed along the [100] direction. The inset is the fast Fourier transform (FFT) from the whole area. The nanocavities have a polyhedral shape. The boundaries between the nanocavities and the nanorod body are sharp. The boundary planes are $\{01\bar{1}\}$ {100}, and {001}, which are all low-index planes of the anatase

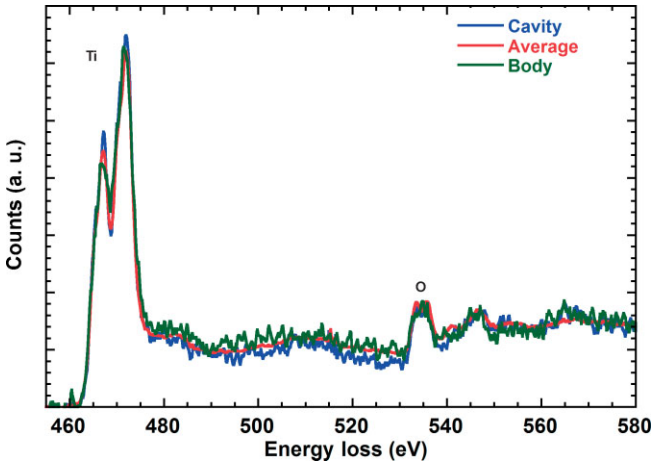

Figure 3. Core-loss EELS spectra from the center of the nanocavity and the body of the nanorod (the positions are indicated by the dots in Fig. 1d). The spectra show the Ti L-edge and the O K-edge. For comparison, an average spectrum, taken at lower magnification is also shown here. It can be clearly seen from the spectra that the Ti intensity is higher in the nanocavity compared to the body and the average spectrum. The spectra were normalized to the intensity beyond the O K-edge. Furthermore, the Ti L_3/L_2 ratio appears to increase in the spectrum taken from the nanocavity compared to the bulk. This indicates that the TiO_2 around the nanocavity is oxygen-deficient, and thus the Ti valence decreases.

crystal and have the lowest surface formation energies, namely, 0.44, 0.53 and 0.90, 26 J m^{-2}, respectively.[10] $H_2Ti_3O_7$ has a monoclinic lattice with $a = 0.8771$ nm, $b = 0.3733$ nm, $c = 0.9759$ nm, and $\beta = 104.42°$.[6c] There are 4 H atoms, 6 Ti atoms, and 14 O atoms in one unit cell, so we use $H_4Ti_6O_{14}$ to represent the unit cell for convenience. Figure 4b and c shows the [010] and [100] projections of $H_2Ti_3O_7$, respectively. There is a tunnel along the [010] direction with a distance of 4 Å between the two nearest oxygen ions. This tunnel provides a channel for gases passing through, such as H_2O, O_2, or Ar. Given that anatase TiO_2 (Fig. 4d) has a tetragonal lattice with $a = 0.3785$ nm and $c = 0.9514$ nm, we use Ti_4O_8 to represent its unit cell as each unit cell has 4 Ti and 8 O atoms. The spacing of (001) and (010) planes in Ti_4O_8 are similar to that of (001) and (010) planes in $H_4Ti_6O_{14}$. However, Ti_4O_8 is much denser than $H_4Ti_6O_{14}$, for example, the volume of 4 $H_4Ti_6O_{14}$ units is close to that of 9 Ti_4O_8. During the transformation of $H_4Ti_6O_{14}$ to Ti_4O_8, 4 $H_4Ti_6O_{14}$ units transform to 6 Ti_4O_8 and 8 H_2O molecules. The evaporation of H_2O leaves empty space, the volume of which equals that of 3 Ti_4O_8. By defining an anti-Ti_4O_8 unit cell, which has the same lattice as that of Ti_4O_8 but without any atoms, the chemical reaction can be expressed as:

$$4\,H_4Ti_6O_{14} \rightarrow 6\,Ti_4O_8 + 8\,H_2O\uparrow \rightarrow 6\,Ti_4O_8 + 3\,\text{anti-}Ti_4O_8 \qquad (1)$$

Hence, we propose an "anti-crystal growth" model, which parallels the classic nucleation theory[11] to explain the formation of nanocavities, that is, "anti-nanopolyhedra". The intermediate product $H_2Ti_3O_7$ was made via the low-temperature, wet-chemistry method and thus contains many defects, such as voids, which are favored places to start an "anti-nucleation" process during the above reaction. The free energy per unit volume favors the formation of the new phase (enlarged voids) while the surface energy (i.e., the surface energy of surrounded cogrowth TiO_2 crystal) disfavors it.[12] In an O_2 background pressure, oxygen-deficient surfaces of TiO_2 react with O_2 (electronegative element) at a specific temperature and thus cause reoxidation and restructuring of the oxygen-exposed surfaces, resulting in lower surface energy.[13] This causes the anti-Ti_4O_8 crystal to nucleate and tend to grow into a nanocavity, as shown in Fig. 4e. On the contrary, Ar (inert gas) does not lower the surface energy and, thereby, prevents the nucleation and growth of anti-Ti_4O_8 crystals. In this case, the nanorods will shrink to remove the unstable small empty space.

Figure 5 shows the molar absorption coefficient (ε) of TiO_2 nanorods with nanocavities when the incident light wavelength (λ) is below 385 nm (close to 3.2 eV of the bandgap of anatase TiO_2); the value of ε is about 25 % higher than that of TiO_2 without nanocavities. In the region where λ is greater than 385 nm, ε of the TiO_2 nanorods with nanocavities is lower than that of TiO_2 without. Since the samples with and without nanocavities have similar shape and size distributions, the cause for the difference in ε in the different λ regions could be attributed to the presence of the nanocavities.

ε has a linear relationship with the effective thickness of the solution. The calculated ε shown in Figure 5 does not include the effect of the nanocavities on the effective thickness of the measured solution. If this effect is considered, the effective thickness of the solution of TiO_2 with nanocavities is smaller than that of the solution of TiO_2 without nanocavities. This explains why the ε of the sample with nanocavities is lower than that of the sample without nanocavities when $\lambda > 385$ nm. The remaining question is how to explain the abnormal result of ε when $\lambda < 385$ nm. Saha and co-workers calculated the effect of nanocavities in Si thin films on the effective optical absorption coefficient. They expected a significant enhancement of ε by introducing nanocavities because of the back-scattered light (Rayleigh scattering for small nanocavities, and the gradual transition from Rayleigh scattering to diffraction phenomena in the case of large nanocavities) effects from the nanocavities.[3] This model can also be used to explain our abnormal optical absorption results. In the high-wavelength region ($\lambda > 385$ nm), the effect of back-scattered light from the nanocavities is not obvious as the size of nanocavities is far less than the light wavelength. The effective thickness plays the major role and thus the calculated ε of the TiO_2 nanorods with the nanocavities is less than the effective ε (the same as the ε of the TiO_2 nanorod without nanocavities). At a lower wavelength range ($\lambda > 385$ nm), however, the size of the nanocavities is close to λ, so the effect of back-scattered light from the nanocavities becomes significant and therefore makes the ε of the TiO_2 nanorods with nanocavities higher than that without nanocavities.

ADVANCED MATERIALS

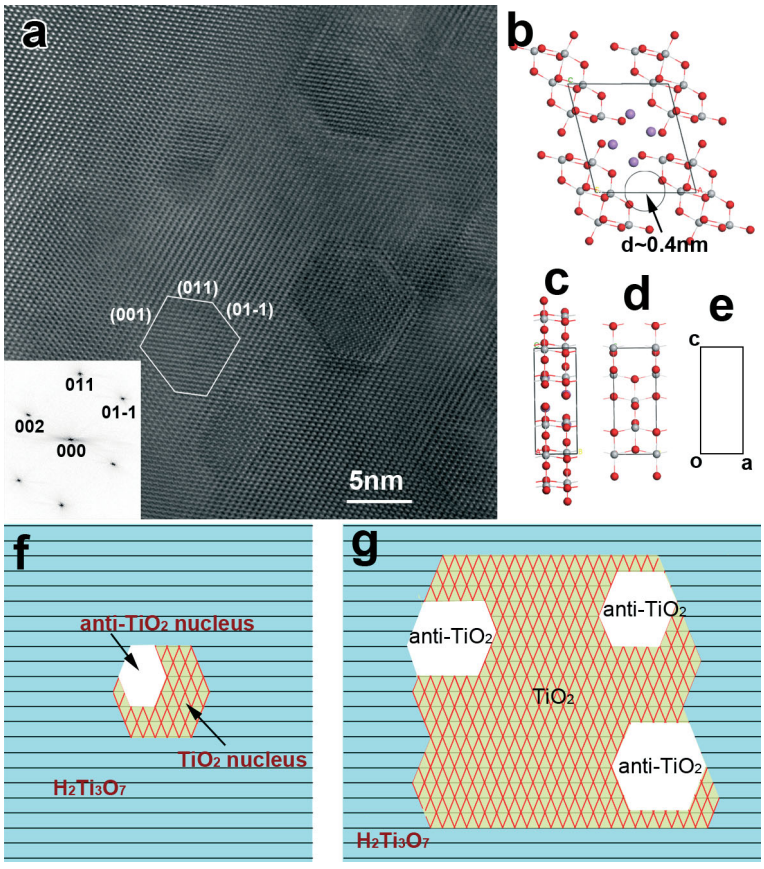

Figure 4. a) High-resolution image viewed along [100] direction, showing polyhedral nanocavities in the nanorod. The inset is the fast Fourier transform (FFT) from the whole image. The surface of the nanocavities are (001), (011), (01$\bar{1}$), and (100) planes. b) [010] projection of the $H_2Ti_3O_7$ structure. The circled area (diameter, $d = 4.02$ Å) could serve as a tunnel for gases to pass through, e.g., H_2O and O_2. c–e) [100] projections of $H_2Ti_3O_7$, TiO_2, and the anti-TiO_2 lattice, respectively. f, g) Schematic drawings of the nucleation (f) and growth (g) of TiO_2 and anti-TiO_2 crystals.

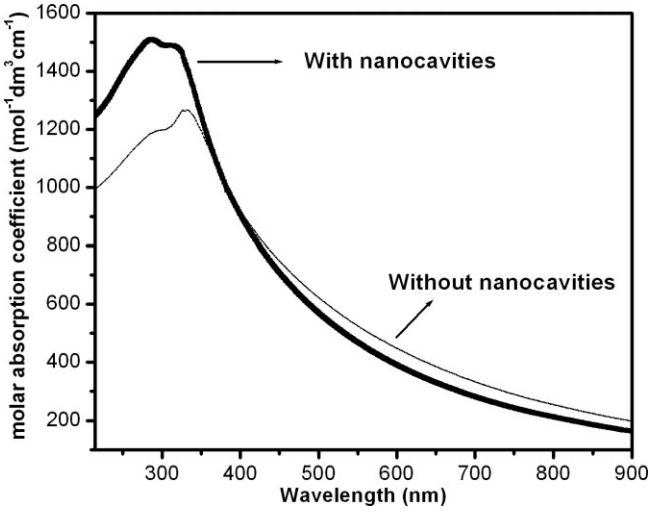

Figure 5. Molar absorption coefficient (ε) versus incident light wavelength (λ) spectra for TiO_2 nanorod samples with and without nanocavities.

The approach we report here to enhance the optical absorption, and thus the photoreactivity, by the introduction of nanocavities, can be extended to other semiconductor nanomaterials. The incorporation of this approach with other approaches, such as doping and metal loading, could make a promising future for TiO_2 to be applied in photoelectrochemical systems.

Experimental

The XRD spectra were performed with Cu Kα radiation on a Rigaku/Miniflex diffractometer. UV-vis spectra were collected on a Perkin–Elmer Lambda 35 spectrometer (200–900 nm). The molar absorption coefficient–wavelength spectra were calculated based on the Beer–Lambert law ($\log I_0/I = \varepsilon lc$, where I_0 = the intensity of the incident radiation; I = the intensity of the transmitted radiation; ε = the molar absorption coefficient; l = the path length of the absorption solution [cm]; c = the concentration of the absorption species [mol dm^{-3}]) from the measured UV-vis absorbance spectra. The analytical TEM results that are presented in this paper were obtained using the JEOL 3000F transmission electron microscope, equipped with an ultra-high-resolution (UHR) objective lens pole piece, an annular dark-field detector, and a post-column Gatan imaging filter (GIF). The instrument is capable of being operated in either the conventional TEM or STEM modes. For the atomic resolution imaging and EELS spectra shown here, the incoherent high-angle annular dark-field imaging (HAADF) mode in STEM was used exclusively. The lens conditions in the microscope and spectrometer were setup with a convergence angle (α) of 11 mrad, a detector inner angle of 30 mrad, and an EELS spectrometer collection angle (θ_c) of 25 mrad. The thickness profile was computed by using the Log-Ration Method as implemented in the Gatan Microscope Suite Program. The EELS spectra were background-subtracted but not corrected for multiple-scattering effects.

Received: March 4, 2007
Revised: April 3, 2007
Published online: August 22, 2007

[1] a) K. Honda, A. Fujishima, *Nature* **1972**, *238*, 37. b) T. Kawai, T. Sakata, *Nature* **1980**, *286*, 31. c) B. O'Regan, M. Gratzel, *Nature* **1991**, *353*, 737. d) Z. L. Wang, *Ann. Rev. Phys. Chem.* **2004**, *55*, 159. e) J. J. Park, S. Kim, A. Bard, *Nano Lett.* **2006**, *6*, 24.

[2] a) S. U. M. Khan, M. Al-Shahry, W. B. Ingler, *Science* **2002**, *297*, 2243. b) M. R. Hoffman, S. T. Martin, W. Choi, D. W. Bahnemann, *Chem. Rev.* **1995**, *95*, 69.

[3] a) M. Banerjee, S. K. Datta, H. Saha, *Nanotechnology* **2005**, *16*, 1542. b) D. Majumdar, S. Chatterjee, M. Dhar, S. K. Dutta, H. Saha, *Sol. Energy Mater. Sol. Cells* **2003**, *77*, 51.

[4] a) P. D. Yang, D. Zhao, D. I. Margolese, B. F. Chmelka, G. D. Stucky, *Nature* **1998**, *396*, 152. b) R. L. Putnam, N. Nakagawa, K. M. McGrath, N. Yao, I. Aksay, S. M. Gruner, A. Navrotsky, *Chem. Mater.* **1997**, *9*, 2690.

[5] a) J. H. Evans, *Nature* **1971**, *229*, 403. b) G. Muller, R. Brendel, *Phys. Status Solidi A* **2000**, *182*, 313. c) H. Seel, R. Brendel, *Thin Solid Films* **2004**, *451–452*, 608. d) W. Q. Han, A. Zettl, *Appl. Phys. Lett.* **2004**, *84*, 2644.

[6] a) T. Kasuga, M. Hiramatsu, A. Hoson, T. Sekino, K. Niihara, *Adv. Mater.* **1999**, *11*, 1307. b) X. Sun, Y. Li, *Chem. Eur. J.* **2003**, *9*, 2229.

c) S. Zhang, Q. Chen, L. M. Peng, *Phys. Rev. B* **2005**, *71*, 014 104. d) R. Ma, Y. Bando, T. Sasaki, *Chem. Phys. Lett*. **2003**, *380*, 577. e) J. Yang, Z. Jin, X. Wang, W. Li, J. Zhang, S. Zhang, X. Guo, Z. Zhang, *Daltron Trans.* **2003**, 3898. f) C. C. Tsi, H. Teng, *Chem. Mater*. **2006**, *18*, 367. g) S. Zhang, L. M. Peng, Q. Chen, G. H. Du, G. Dawson, W. Z. Zhou, *Phys. Rev. Lett*. **2003**, *91*, 256 103. h) G. H. Du, Q. Chen, R. C. Che, Z. Y. Yuan, L. M. Peng, *Appl. Phys. Lett.* **2001**, *79*, 3702. i) Q. Chen, W. Zhou, G. H. Du, L. M. Peng, *Adv. Mater.* **2002**, *14*, 1208. j) Q. Chen, G. H. Gu, S. Zhang, L. M. Peng, *Acta Cryst. B* **2002**, *58*, 587.

[7] a) C. C. Tsai, H. Teng, *Chem Mater.* **2004**, *16*, 4352. b) R. Yoshida, Y. Suzuki, S. J. Yoshikawa, *Solid State Chem.* **2005**, *178*, 2179. c) Y. Mao, S. S. Wong, *J. Am. Chem. Soc.* **2006**, *128*, 8217.

[8] a) S. J. Pennycook, L. A. Boatner, *Nature* **1988**, *336*, 565. b) R. F. Loane, P. Xu, J. Silcox, *Ultramicroscopy* **1992**, *40*, 121.

[9] a) A. Ohtomo, D. A. Muller, J. L. Grazul, H. Y. Hwang, *Nature* **2002**, *419*, 378. b) R. F. Klie, N. D. Browning, *Appl. Phys. Lett.* **2000**, *77*, 3737.

[10] U. Diebold, *Surf. Sci. Rep.* **2003**, *48*, 53.

[11] M. Volmer, *Kinetik der Phasenbildung*, Steinkopff, Dresden and Leipzig, Germany **1939**.

[12] D. W. Oxtoby, *Acc. Chem. Res.* **1998**, *31*, 91.

[13] H. Onishi, Y. Iwasawa, *Phys. Rev. Lett.* **1996**, *76*, 791.

